Mechanisms of root reinforcement in soils

Bull, D. J.; Smethurst, J. A.; Sinclair, I.; Pierron, F.; Roose, T.; Powrie, W.

Published in:
Proceedings of the Royal Society A: Mathematical, Physical and Engineering Sciences

DOI:
10.1098/rspa.2019.0838

Publication date:
2020

Mechanisms of root-reinforcement in soils: an experimental methodology using 4D X-ray computed tomography and digital volume correlation

D.J. Bull[1,*], J.A. Smethurst[1], I. Sinclair[1], F. Pierron[1], T. Roose[1], W. Powrie[1], and A.G. Bengough[2,3]

[1]Faculty of Engineering and Physical Sciences, University of Southampton, United Kingdom
[2] School of Science and Engineering, University of Dundee, Dundee, United Kingdom
[3] The James Hutton Institute, Dundee, United Kingdom
* Corresponding author: daniel.bull@soton.ac.uk

Keywords: Direct shear, slope stability, root reinforcement, digital volume correlation, X-ray computed tomography, soil science

Abstract

Vegetation on railway or highway slopes can improve slope stability through the generation of soil pore water suctions by plant transpiration and mechanical soil reinforcement by the roots. To incorporate the enhanced shearing resistance and stiffness of root-reinforced soils in stability calculations, it is necessary to understand and quantify its effectiveness. This requires integrated and sophisticated experimental and multiscale modelling approaches to develop an understanding of the processes at different length scales, from individual root-soil interaction through to full soil-profile or slope scale. One of the challenges with multiscale models is ensuring that they sufficiently closely represent real behaviour. This requires calibration against detailed high-quality and data-rich experiments. This study presents a novel experimental methodology, which combines *in situ* direct shear loading of a willow root reinforced soil with X-ray computed tomography to capture the 3D chronology of soil and root deformation within the shear zone. Digital volume correlation (DVC) analysis was applied to the computed tomography (CT) dataset to obtain full-field 3D displacement and strain information. This paper demonstrates the feasibility and discusses the challenges associated with DVC experiments on root-reinforced soils.

1 Introduction

Slope instability presents a major hazard to buildings and infrastructure, in the form of large natural landslides and smaller scale failures in engineered slopes. Failure is often associated with prolonged periods of heavy rainfall, which increases pore water pressures and reduces the soil effective stress. Vegetation is a cost-effective method of improving slope stability and reducing the risk of slope failure. The planting of trees, shrubs and grasses on slopes provides a potential increase in the available soil shear strength through a reduction in pore water pressures as plants transpire water, and mechanical root reinforcement of the soil [1-3].

Root reinforcement has been shown to enhance soil shear strength in both laboratory and field tests including direct shear [4-10] and centrifuge model experiments [7, 11-14]. These tests are often supplemented with additional measurements such as root tensile strength [7, 15-17], root pull-out resistance [18] and root distribution/density [19, 20]. While these experiments have demonstrated the effectiveness of root reinforcement on soil, they have not resulted in a full understanding of the complex root reinforcement mechanisms and soil-root interaction during shear, which are difficult to capture as they occur unseen within the body of the soil.

The mechanism of root reinforcement has many contributing factors. These include variables relating to the plant roots (geometry, orientation, density, stiffness, strength, and root-soil interface properties) and soil characteristics (particle size distribution, compaction density, water content, etc.). The many parameters influencing these processes make it challenging to fully understand the behaviour of soil-root interaction and how roots stabilise the soil [12, 21]. Obtaining a better understanding of this behaviour is important for the development of accurate analytical models that will ultimately aid in optimising plant species and their placement for given ground conditions including soil type, slope height and angle. While many models have been developed for soil-root interaction, most have relied on simple empirical relationships or made assumptions due to a lack of experimental data [22].

There have been recent attempts to increase the level of detail and understanding from experimental shear-box and centrifuge tests to quantify the effectiveness of roots in increasing soil shear strength. These include 2D imaging using cameras to capture behaviour on a cross-section of soil through a transparent window, from which displacement and strain information were obtained using digital image correlation (DIC) or particle tracking approaches [12, 23, 24]. A limitation of this technique is that it can only make observations of the surface plane, where soil movements could be influenced by boundary effects such as friction, shear and variations in soil compaction adjacent to the window. It is also challenging to capture features such as soil-root interaction, which may not take place directly on the observed surface.

To capture the three-dimensional behaviour of the soil and soil-root interaction, it is necessary to obtain information from within the bulk of the soil. Advances in X-ray computed tomography (CT) have been shown to work well for capturing 3D information within soils (including roots) and have led to a considerable increase in its use in soil science within the past decade. Interrupted (while CT scanning takes place) *in situ* experiments on soils have been carried in a small number of studies to understand the mechanics of soil (such as dilation and bifurcation behaviour) and soil-root behaviour during root growth. These studies have applied digital volume correlation (DVC), a technique similar to digital image correlation (DIC), to obtain 3D full-field displacement and strain information in the bulk, but have so far been limited to specimens less than 50 mm in diameter [25-27]. To the authors' knowledge, there are no published studies applying DVC to study the effects of direct shear on root-reinforced soils.

The research presented here combines direct shear experiments *in situ* with X-ray CT to understand and quantify the 3D soil mechanics and soil-root interactions in response to a direct shear load. The study explores the feasibility of this experiment at a larger scale (field of view: 80 mm × 80 mm × 80 mm) than used before (both at the University of Southampton and elsewhere) on soil containing clay, silt and sand particles up to 2 mm in size, representing a suitable growth medium for plants. This research establishes a methodology for conducting such experiments, which can be applied to more extensive studies.

2 Experimental design philosophy

The development of the experimental test rig and methodology for carrying out and analysing the results from the experiments required careful consideration and design. Sections 2.1 to 2.3 describe the overarching principles and decisions that guided the final experimental design. This leads into the experimental procedures explained in more detail in sections 3, 4 and 5, which cover the design of the shear box apparatus, experimental methodology (soil and plant preparation, and X-ray CT procedure) and digital volume correlation procedure, respectively.

2.1 Plant and soil selection

Willow plants were used to provide root architectures for this study. Owing to its fast growth and high demand for water, willow is often considered in planting schemes for slope stability [3, 7], and has also been used in parallel experiments carried out at the University of Dundee [7, 13]. The soil used in the experiments needed to be able to support plant growth, and was selected based on its prior use in similar experiments [7, 13]. Soil specimens were sheared unsaturated, which negated the need for the water bath commonly used to saturate samples in a conventional soil mechanics shear box, which would be difficult to accommodate in the CT scanner.

2.2 Height and size of rooted soil specimen

The specimen needed to be sufficiently large to allow the willow plant to develop a reasonable root structure and provide good root anchorage into the upper and lower portions of the sample. This leads to the use of tall samples (0.5 m), similar to other root shear studies [7, 13]. The diameter of the sample needed to balance the requirements for an adequate shear test with the ability of X-rays to penetrate the specimen and provide enough image resolution. The X-ray CT process rotates the specimen through 360 degrees to form an image. It is desirable for image quality (noise, artefacts, etc.) to have a uniform X-ray cross-section, hence (unconventionally for direct soil shear tests) cylindrical soil specimens were used. CT scanning the full sample from top-to-bottom presents significant challenges to rig design, where placement of non-uniform volumes of metal (connecting brackets etc.) within the X-ray field of view makes it difficult to maintain image quality. It was therefore decided to concentrate on imaging the sample shear zone (~ 80 x 80 x 80 mm region of interest). The use of a tall sample requires long (two months) root growth periods thus the apparatus needed to allow samples to be grown out of the rig and mounted into it for shearing; growing samples in the apparatus e.g. [28] would be too time consuming.

Many plants will not grow roots to particularly large depths in the field (beyond ~1 m for grasses and small shrubs), hence the zone of greatest root reinforcement is close to the ground surface at low total vertical stresses. It was therefore decided that the application of a vertical stress to the top of the soil sample was not required, hence no provision was made to load the sample vertically. Thus only modest forces (<200 N) would be needed to shear the sample, and the rig could be small enough in mass (<20 kg) and size (<400 mm diameter) to fit within a CT scanner.

2.3 Imaging and analysis approach

X-ray imaging of the rooted soil specimen introduces several challenges. The physical diameter of the specimen in conjunction with the size of soil particles and maximum shear displacement needs to be balanced against the CT field-of-view, voxel resolution, image quality (contrast-to-noise ratio), scan time and the digital volume correlation (DVC) process.

Sufficient resolution and contrast-to-noise ratios are needed to capture the major roots of the willow plants, and soil particles up to 2 mm in diameter. This is important for the DVC process, which matches subsets of voxels to determine displacement and strain, where imaging features (*e.g.* the soil particles) are required to accurately track the positions of the subsets, and where the DVC process (*e.g.* displacement and strain noise) is sensitive to the CT volume quality (e.g. contrast-to-noise and spatial resolution of features) [29]. Further, there is a trade-off between CT resolution and field-of-view, *i.e.* increasing the size of the field-of-view reduces the resolution. For the direct shear experiments, the field-of-view and its corresponding resolution also needed to be balanced against the maximum shear displacement of the specimen. As the specimen is sheared, features that move out of the field-of-view are lost, reducing the remaining size of volume that is captured and can be processed with DVC.

Considering these limitations, the first step was to decide on an appropriate diameter for the rooted soil specimen. The specimen needed to have a large enough diameter to allow a reasonable shear displacement to be applied; however, this had to be balanced with the impact it has on other aspects of the CT scan. The diameter of the specimen has a direct effect on both X-ray transmission and sample positioning within the cone beam geometry of the CT scanner. A larger diameter requires more X-ray power to penetrate the specimen, which can be detrimental to spatial resolution owing to the effects on X-ray target spot size if high energies are needed [30]. A larger diameter sample must be positioned further from the X-ray source, which can be detrimental to the image resolution and signal-to-noise in the volumes obtained.

Considering these trade-offs, a sample diameter of 110 mm was chosen with a local CT scan applied to achieve a useable field-of-view approximately 80 mm × 80 mm × 80 mm at 46 µm voxel resolution. This was sufficient to detect the soil particles and larger plant roots (>1.5 mm diameter). The field-of-view enabled a maximum shear displacement of 20 mm.

3 Development and construction of the shear apparatus

A bespoke test rig was manufactured for the *in situ* direct shear testing of a willow rooted soil specimen within the X-ray CT scanner (Figure 1 and Figure 2). The rig was designed to enable full control of the applied direct shear displacement while also monitoring load, displacement and tensiometer sensors from outside the CT scanner. Two Arduino Uno microcontrollers were used for the test rig: one positioned on the test rig to connect to sensors and the stepper motor controlling shear displacements, and another outside the CT scanner which transferred sensor data to a MATLAB data acquisition script and acted as the master controller for operating the stepper motor. A wired connection was used to pass data between the two Arduinos using an I^2C protocol.

The test rig consists of a lower saddle bracket mounted on two horizontal rails with one degree of freedom which is moved by the stepper motor with the displacement monitored using a linear variable differential transformer (LVDT) displacement sensor. The lower bracket is attached directly to the lower half of the specimen tube and controls the shear displacement applied to the sample. The upper section of the specimen is fully constrained in a bracket mounted to a load cell, measuring reaction force.

To facilitate use in an X-ray CT scanner, the support frame needed to provide a uniform X-ray path length hence uniform attenuation during the 360 degrees of rotation. To achieve this, the rig has a cylindrical aluminium support (of height 152 mm and wall thickness 3.3 mm) surrounding the specimen shear plane, which was the main zone of interest for imaging root-soil interaction. The cylindrical aluminium section also acts as an X-ray filter, pre-hardening the X-ray beam and reducing the extent of beam hardening on CT reconstructions [31].

The diameter of the aluminium support cylinder (356 mm) is large enough to provide clearance for mounting the test specimen (including access for tools and hands), but small enough to allow adequate X-ray resolution and signal-to-noise during the CT scan. A smaller diameter support tube enables closer positioning of the specimen to the X-ray source. This has two benefits: (1) reducing the X-ray source to object distance, which improves the voxel resolution that can be obtained, and (2) if the desired voxel resolution is exceeded when the specimen is positioned close to the X-ray source, it is possible to reduce the source-to-detector distance to improve flux and subsequently the signal-to-noise ratio, enabling shorter scan times [32]. A series of initial tests was carried out in the CT scanner with a cylindrical aluminium section placed around a prepared soil specimen, to ensure

an optimal compromise was achieved between scan resolution/quality and physical access to the specimen when mounted in the rig.

Above and below the scanning region of interest, the upper and lower saddle brackets holding the two halves of the sample are connected to the top and bottom of the aluminium cylinder using a frame made of square section aluminium lengths (Figure 2). The same frame extends down to a circular aluminium plate connected to the rotating stage within the CT scanner.

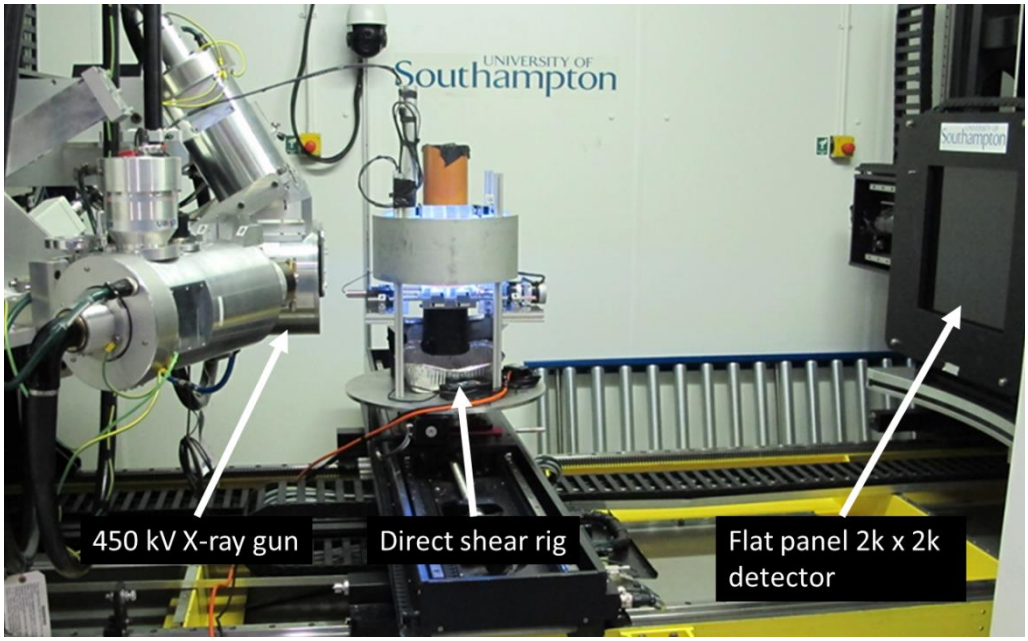

Figure 1: Shear rig set up within the 450kV Hutch X-ray CT scanner at the University of Southampton. The shear rig contains force, displacement and soil tensiometer instrumentation, and is controlled and monitored from outside the CT scanner.

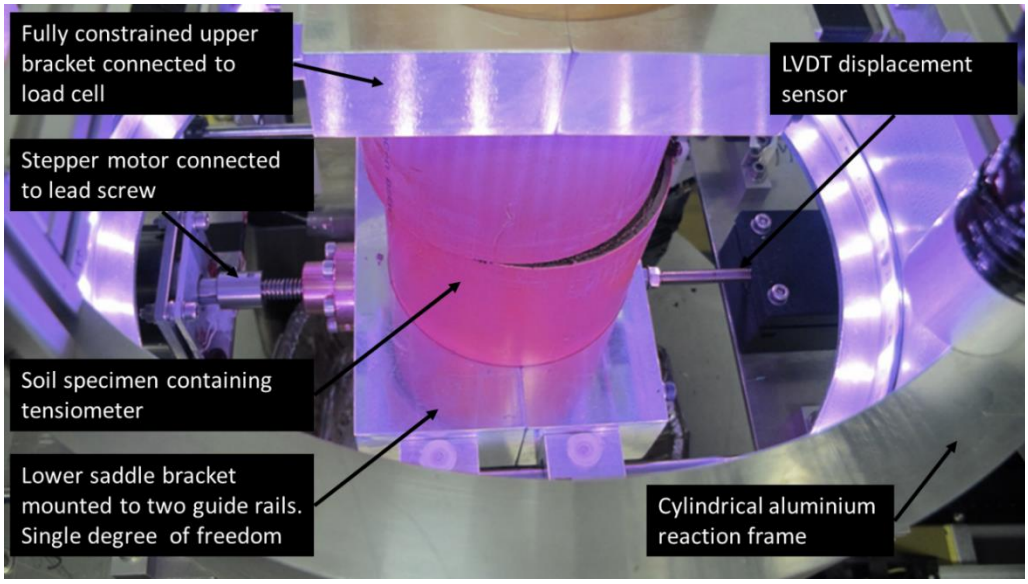

Figure 2: in situ shear rig setup; view looking down at the specimen shear plane through the top of the apparatus.

4 Experimental methodology

4.1 Soil and willow plant preparation

A 110 mm diameter, 500 mm long cylindrical tube was used to prepare each test specimen. The tube comprised two 250 mm length sections, forming a plane at the middle where controlled direct shear could be applied. A 2 mm gap was left between the two tubes which were supported in position using a purpose-made 3D printed bracket. The base of the tube was covered with a permeable membrane.

The willow (*Salix viminalis*, variety Tora) specimen was prepared using Bullionfield soil (71% sand, 19% silt and 10% clay, James Hutton Institute, Dundee, UK) having a pH of 6.2. The soil was oven dried at 60°C for 48 hours and sieved to ≤2 mm grain size. De-aired water was added to achieve a water content of 0.18 gg^{-1}. The soil was compacted in 10 equal layers (50 mm thick) to achieve a target bulk dry density of 1.4 Mg/m^3, which was chosen to ensure that the soil volume was stable under repeat watering, but not too dense to prevent penetration of the plant roots. A single prepared willow cutting, 150 mm long and between approximately 10 mm and 15 mm in diameter, was pushed into the centre of each tube, so that about 75 mm was below the soil surface. The willow plant was grown for 60 days under controlled lighting (operating 16 hours per day), temperature (21°C) and relative humidity (41%). Lighting was provided by a Maxibright T5 unit, equipped with eight blue T5 fluorescent tubes delivering 4450 lumens of light per tube. The height of the lights was adjusted during the growth period to maintain a ~150 mm distance between the lights and tallest part of the plant. The growth period and conditions were sufficient for the willow plants to root to the full depth of the specimen tube (500 mm).

Immediately prior to carrying out the direct shear tests, specimens were fully immersed in water before being placed on a saturated bed of sand within a large container. Water was drained from the bottom of the container resulting in a water table in the sand 0.5 m below the shear plane of the specimen, and an inferred pore water suction of 5 kPa at the shear plane. Prior to shearing, a sharp blade of depth 2 mm was run around the perimeter of the tube at the level of the shear plane to cut any roots directly in contact with the inside wall of the specimen tube.

4.2 Development of the X-ray computed tomography procedure

4.2.1 X-ray CT scan parameters

X-ray CT scans were undertaken using the µ-VIS facility at the University of Southampton, UK, using a large Nikon Metrology Hutch CT scanner. To provide enough X-ray transmission through the rig and specimens, a 450 kV X-ray gun was used. Several trial scans were performed to determine the optimum scan setting giving minimal noise, a fast scan time and good spatial resolution, which can be affected by the increasing X-ray spot size at high X-ray power. The scan parameters determined from the trials are shown in

Table 1.

Table 1. X-ray CT scan parameters for in situ shear testing

CT scan parameter	**Value**
Voltage	300 kV
Power	90 W
Voxel resolution	46 µm
Field of view	80 x 80 x 80 mm
Number of projections	3142
Source to object distance	359 mm

Source to detector distance	1546 mm
Frames per projection	4
Exposure time	134 ms
Analogue gain	24 dB
Scan time	30 minutes
Filtering	6.6 mm aluminium (total transmission through wall thickness from cylindrical support on test rig)

4.2.2 Mitigating soil movement during CT scans

One of the key challenges with obtaining reliable X-ray CT images is ensuring no movement of features within the object during the CT scan. Any movement during the scan can lead to motion artefacts in the reconstructed images, and potentially poor image correlation in the digital volume correlation (DVC) process. To investigate this, trials were carried out in which willow specimens were held at a fixed displacement and the force-time profile measured.

Figure 3 shows a gradual drop in stress when a specimen is held at a fixed displacement after an incremental displacement step was applied. Only the first two displacement steps are shown for clarity, out of seven displacement steps. The steepest portion of the stress relaxation curve occurs in the first 30 minutes, with ~90% of the final stress reduction occurring in this period. The displacement sensors indicated no external movement while loading was paused, hence it is conjectured that the loss in stress was due to internal relaxation of the roots.

In all experiments, a 30-minute wait period was implemented between the end of shearing and commencement of CT scanning. While a longer wait period might be desirable, it is important to consider also the restriction this would have imposed on the number of displacement steps that could have been completed within a 12-hour X-ray CT scan session.

Figure 4 shows that any shear stress lost in the relaxation period was quickly regained on restarting direct shearing. Tests where shearing was carried out with continuous loading were compared with those in which shearing was repeatedly interrupted for CT scanning. These showed no differences beyond that expected due to the variation of the biological (root) content of the specimens. The shear stress obtained with willow was larger than for fallow specimens, which gave critical states (shearing at constant shear stress, and volume) consistent with a soil friction angle of 36° [7].

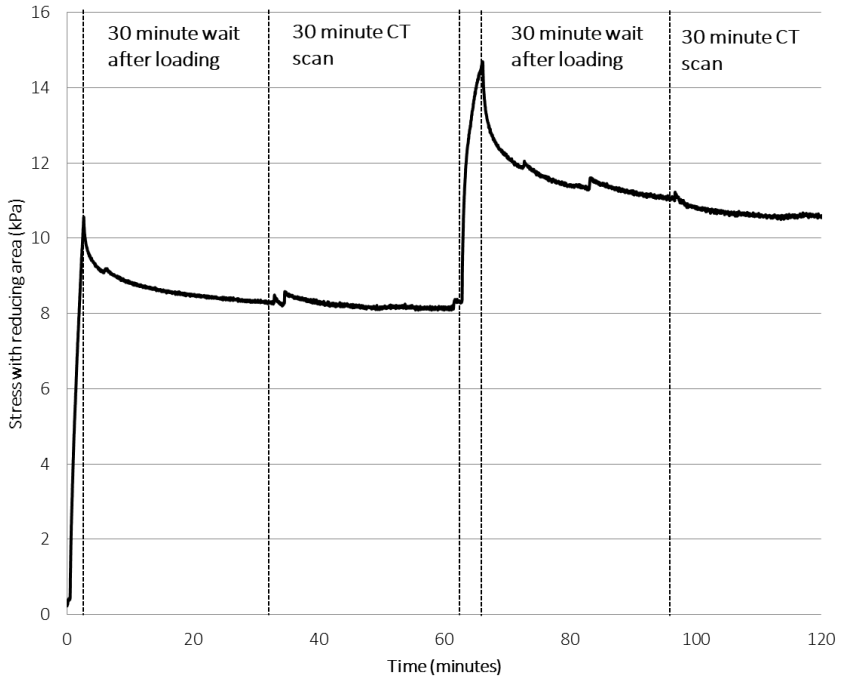

Figure 3: stress relaxation plot for a willow specimen held at two fixed shear displacements (1.72 and 4.87 mm respectively).

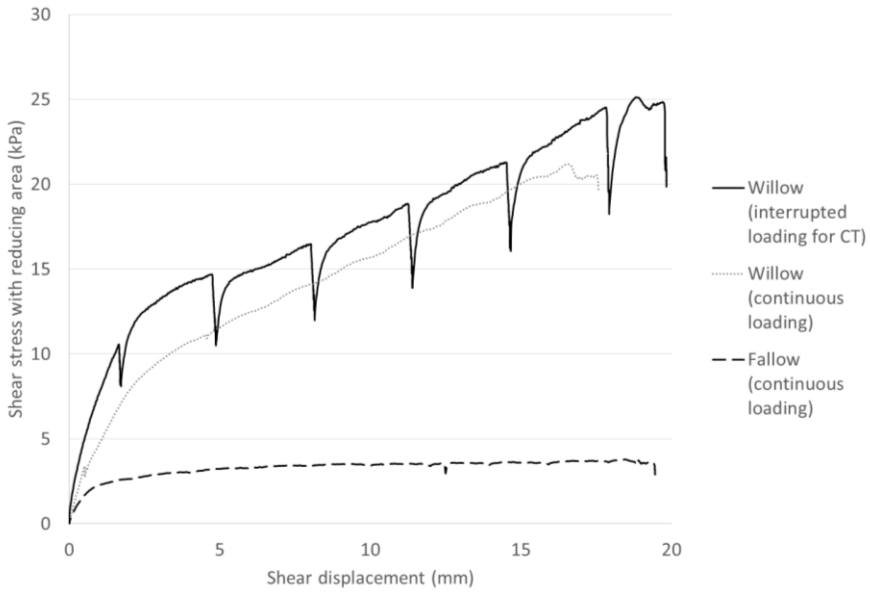

Figure 4: shear stress and shear displacement data showing Willow loaded with interruptions and continuously and an unrooted fallow specimen for comparison.

4.2.3 *In situ* CT direct shear experiments

Once the desired scan parameters were determined, the scan procedure for the *in situ* shear box experiment consisted of four noise study scans, and eight scans associated with the application of shear displacement steps. The noise study scans applied various known displacements to the sample to evaluate the performance of digital volume correlation and its sensitivity to noise. These consisted of two stationary scans, one rigid body motion scan (moving the specimen 1 mm vertically up) and a zoom out scan (moving the specimen 1 mm away from the X-ray source). Eight scans were conducted for each shear experiment. These consisted of an unloaded CT scan followed by seven

scans, each after an incremental shear displacement of 1.7 - 3.3 mm had been applied to the sample.

5 Digital volume correlation (DVC) noise study

To obtain accurate displacement and strain data from DVC, it is necessary to choose an appropriate experimental procedure (scan settings, size of shear displacement steps) and DVC parameters such as subset size to evaluate their effects on spatial resolution and noise.

5.1 DVC processing

DVC was applied to the X-ray CT datasets to obtain full-field volumetric displacements and strains during *in situ* shear loading. Full details of the DVC analysis parameters are shown in Table 2. Data were processed using DaVis LaVision 8 software. Processing involves correlating sub-volumes within a deformed volume against a reference volume to calculate local displacements, and subsequently derive strain information. Matching between sub-volumes was carried out using a coarse Fast Fourier Transform (FFT) correlation step to create an initial predictor of the displacement field, followed by a more accurate Direct Correlation (DC) step.

An adequate subset size was selected to achieve a balance between the error caused by noise, reliable correlation, strain measurement accuracy and spatial resolution. The first stage was to perform a noise sensitivity study to evaluate the strain measurement resolution [33] and determine the minimum significant strain value that can be extracted from the deformed images.

DVC is not able to correlate between successive volumes if the deformations are too large [33]. For the incrementally displaced specimens, trials were conducted to establish how well the deformed volumes could be correlated. This may be carried out via two approaches: (1) reference to first scan and (2) sum of differential between scans. The reference to first approach keeps the first volume in a time series as the reference, while the sum of differential approach makes use of the intermediate displacement steps by comparing sequential pairs in the time series before summing together the displacement fields. The trials found that it was necessary to apply a sum of differential approach instead of the reference to first method, owing to the large applied displacements and deformations in the dataset. One of the downsides of using the sum of differential approach is that noise in each volume is progressively summed together. It is therefore important to understand the level of noise associated with the number of displacement steps.

Table 2: DVC analysis parameters

DVC Software	Davis LaVision, Version 8
Image Filtering	Gaussian filter with a 3x3x3 pixel kernel
Subset sizes	32^3, 48^3, 64^3, 96^3, 128^3 pixels^3 1.47^3, 2.21^3, 2.94^3, 4.42^3, 5.89^3 mm^3
Noise for 32^3 pixels^3 subset size	Displacement noise: 5.4 µm Strain noise: 6.8 millistrain
Subset step size	75% overlap
Subset Shape Function	Affine
Matching Criterion	Cross-correlation (CC)
Interpolant	Spline 6
Strain Window	3 data points
Virtual Strain Gauge Size	192, 144, 96, 72, 48 pixels 8.8, 6.6, 4.4, 3.3, 2.2 mm
Strain Formulation	Green-Lagrange

5.2 Noise study: choice of DVC subset size

For the noise study, five subset sizes with 75% overlap were identified with varying isotropic sub-volumes of dimension: 128, 96, 64, 48, and 32 pixels. In addition to the specific rigid body tests, *in situ* shear displacements were also assessed in terms of far-field strains to confirm noise levels. To give an appreciation of the size of the subset relative to the volumetric CT scan, Figure 5 shows an overlay of the subsets over a cross-sectional slice from the willow X-ray CT scan.

The first set of noise study scans (stationary, rigid body motion and magnification) were used to determine the level of noise with a controlled/known level of strain. In the stationary and rigid body motion cases, the expected strain is zero. The stationary case studied the effect of sensor noise and CT artefacts like scattering, while rigid body motion provided a more realistic noise test as the grey level interpolation was also assessed. However, rigid body motion only provides a spatially constant interpolation bias. For a more realistic case, a change of magnification test was carried out, in which the images were 'optically deformed', to simulate a triaxial state of uniform strain. This tests all of the contributions to the displacement and strain uncertainties. The change of magnification gave an artificially introduced uniform level of strain (12 millistrain) across the full volume. The standard deviation of strain obtained from the change in magnification test provided a strain noise floor that would be closely representative of the *in situ* displacement tests.

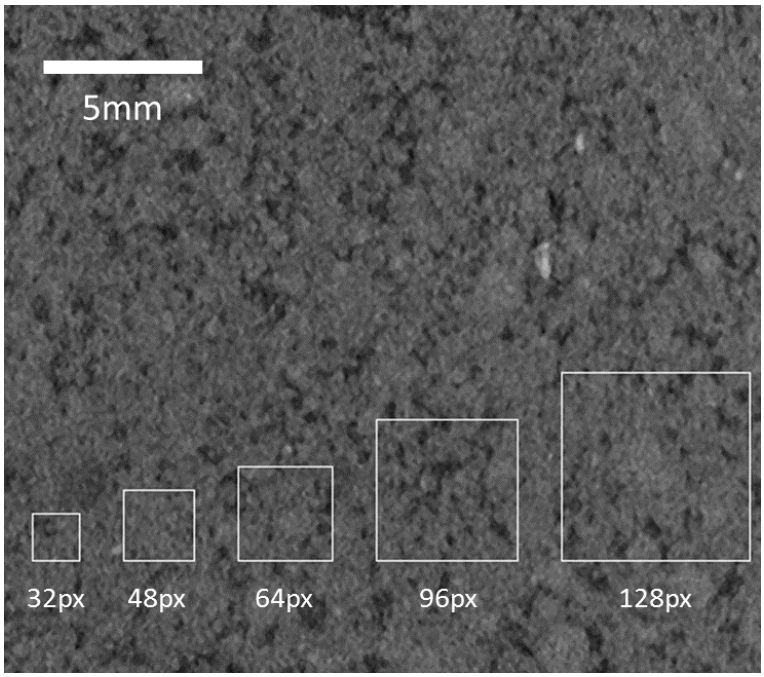

Figure 5: subset sizes (32 to 128 pixels) shown on a cross-sectional slice from the willow X-ray CT scan

Directional dependencies to noise, may be assessed by considering the three orthogonal component normal strains ε_{xx}, ε_{yy} and ε_{zz} and displacement vectors v_x, v_y and v_z. Figure 6 shows the standard deviations of strain from a cropped subset volume three subsets away from any scan or object boundary to remove edge effects. There are several important observations from the noise study scan data:

(1) There is no significant directional dependency on strain, with all three orthogonal standard deviation strain components (ε_{xx}, ε_{yy} and ε_{zz}) giving the same level of noise across all subset sizes and scan types tested. This was also true for the displacement vectors.

(2) There is a diminishing return in terms of noise reduction from increasing the subset size.

(3) For subsets less than 64 pixels, the level of strain noise is unaffected by the type of noise scan (stationary, rigid body motion and magnification). For subsets greater than 64 pixels, the magnification strain noise floor is more than twice that of the stationary and rigid body motion cases.

(4) The level of noise at the smallest subset size tested (32 pixels) approaches 7 millistrain.

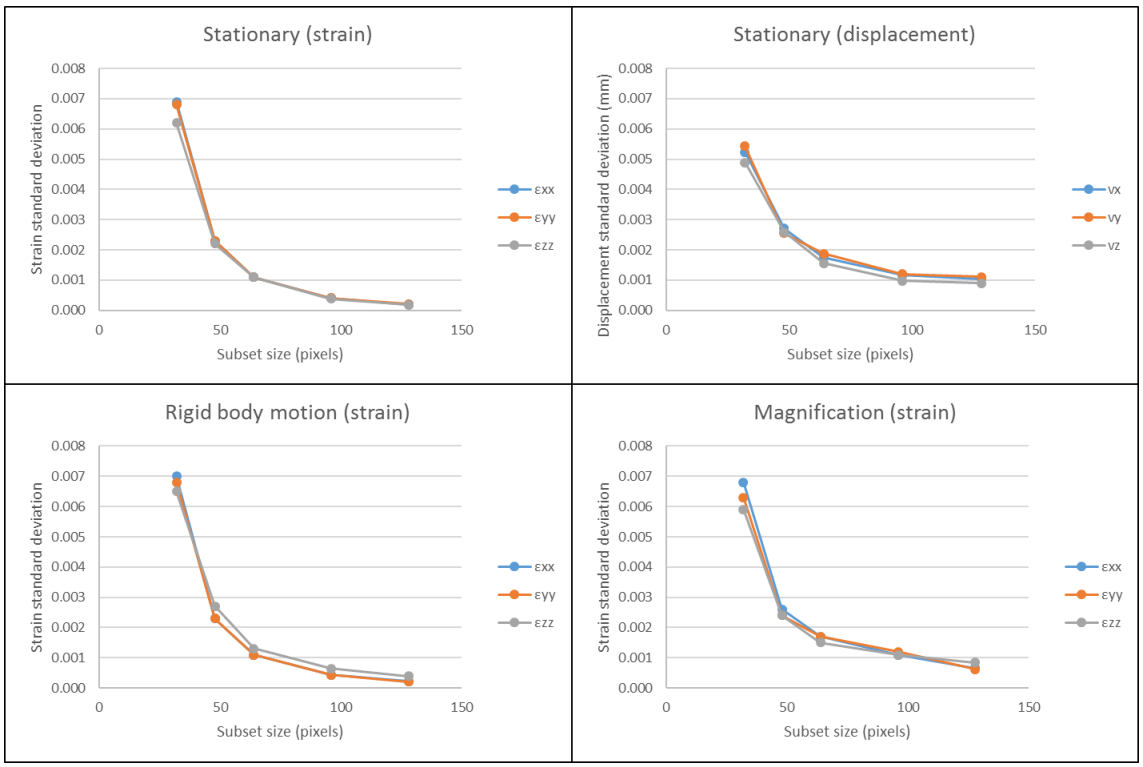

Figure 6: DVC noise study showing standard deviation of Green-Lagrange strains for stationary, rigid body motion and magnification CT scans at five different subset sizes.

Figure 6 shows the effects of noise under a controlled set of noise scans. The *in situ* shear test adds complexity that is not captured in these noise scans. These can include scan to scan variations over a long test period, potential changes in soil conditions over time and the effects of using the sum of differential approach which sums noise with each displacement step. To assess the level of noise in the *in situ* scans, the strain standard deviations were calculated using the far-field strains in the shear test volume well away from the shear zone. The plots in Figure 7 show the strain standard deviation (solid lines) as a function of the current load for different subset sizes. For comparison, the mean strains within the sampled region are also plotted. Each plot contains data representing each strain component: ε_{xx}, ε_{yy}, ε_{zz}, and ε_{xz}. The displacement steps 2 to 8 correspond to an increasing level of shear displacement: 1.72, 4.87, 8.15, 11.39, 14.69, 17.93 and 19.83 mm respectively as measured by the displacement sensor.

ε_{xx} and ε_{yy} show a strong linear trend in the standard deviation of strain with increasing number of displacement steps (R^2>0.99) for all subset sizes. This linear behaviour is unaffected by the non-uniform spacing between shear displacements, *e.g.* between steps 5, 6, 7 and 8 the incremental shear displacements are 3.3, 3.2 and 1.9 mm respectively. Therefore, the noise is dominated by the number of displacement steps in the sequence owing to the sum of differential approach used to calculate strain. The scaling of noise highlights a particular problem when designing the *in situ*

experiment. If too many displacement steps are generated, the noise floor could rise to levels where strain signals can no longer be detected.

A non-linear trend to strain standard deviation is apparent in the ε_{zz} and ε_{xz} strain components. In these cases, some real strain signals were sampled, represented by the drift in the mean strain measured. Hence, the standard deviation of strains would overestimate the level of noise. Nonetheless, the largest strain standard deviation was observed in ε_{xx} representing 38 millistrain on the final displacement step with a 32 pixel subset size.

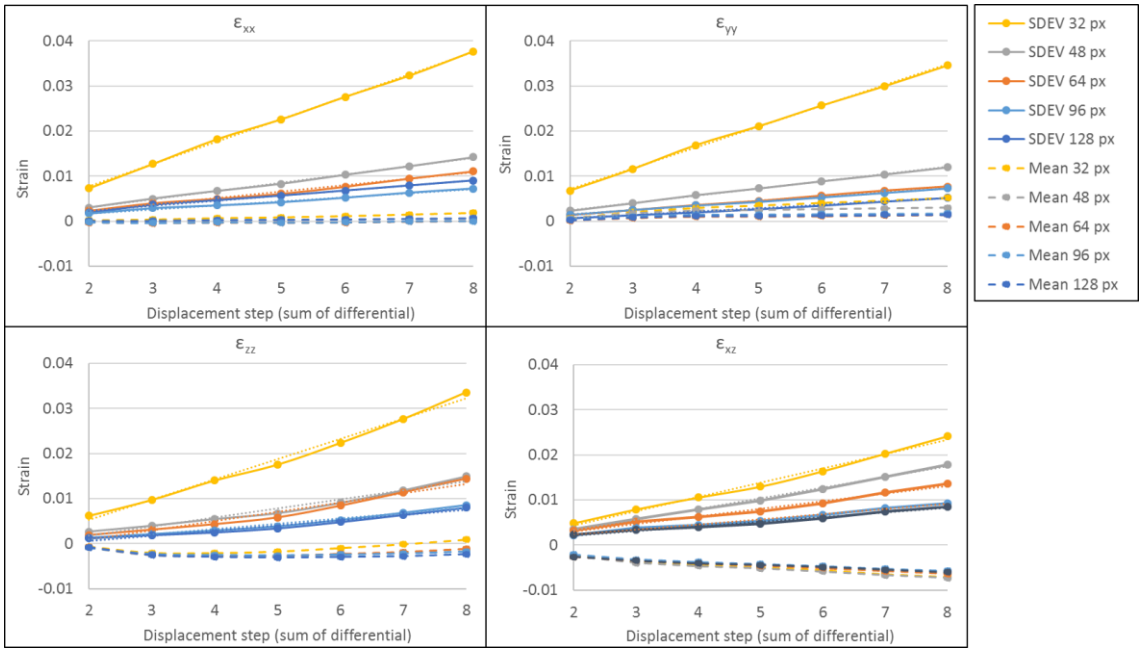

Figure 7: Plots showing standard deviation (SDEV) of far field- strains (solid lines) against applied displacement step for different subset sizes. The plots act as a representation of strain noise present during the direct shear experiment which is shown to increase with each applied displacement step caused by the sum of differential approach in the DVC process. For comparison, the mean strain values are also plotted (dashed lines).

Figure 8 indicates the effects of subset size on the spatial resolution of volumetric strains ($\varepsilon_{volumetric} = \varepsilon_{xx} + \varepsilon_{yy} + \varepsilon_{zz}$). The images show a cross-sectional view through the middle of the specimen at the final displacement step for subset sizes ranging from 128 to 32 pixels. Due to the presence of strain gradients and local strain concentrations in the full-field dataset, the effects of reducing the subset size are clear. The level of detail captured around local events is averaged out and "smeared" with larger subset sizes, and the magnitude of strains around localised strain concentrations averaged down. This is evident in the tagged region indicated in Figure 8 as a localised strain concentration feature which shows increasing localised volumetric strain values (0.10 to 0.72) with decreasing subset sizes (128 to 32 pixels) respectively. It was decided to use the smallest subset size possible to capture these local details taking into consideration the increase in the level of noise.

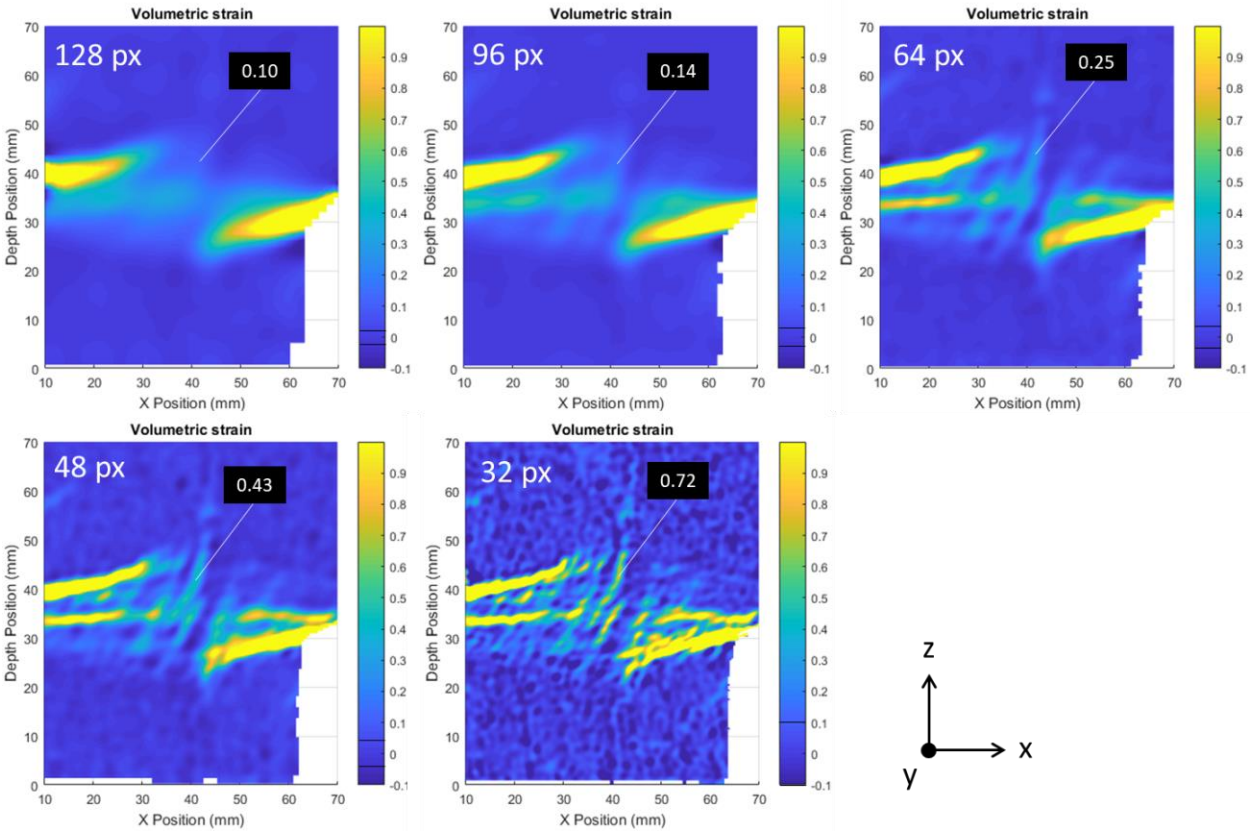

Figure 8: Effects of subset size on spatial resolution and detection of local magnitudes of strain. Volumetric strains are the sum of ε_{xx}, ε_{yy} and ε_{zz} normal strains. Strain standard deviation is indicated on colour bars for each subset size. A tag indicates a localised strain concentration which is underrepresented with larger subset sizes.

6 Results and discussion

This section presents results from shear tests carried out on a willow root reinforced soil specimen. The purpose is to demonstrate the overall experimental design and approach, and to discuss how these results could be used to help understand soil-root interaction for use in analytical models. The direct shear results could be used with complementary experiments and datasets such as root counts, mechanical testing of individual roots (for root stiffness and strength) and conventional direct shear tests on fallow samples (to give soil stress-displacement curves) [7].

6.1 Local behaviour

The typical cross-sectional view of the X-ray CT scan in Figure 9 shows the level of detail of features captured within the scan volume. The CT scan can capture soil grains and roots larger than 1.5 mm diameter (circled) that run near-vertically down the length of the tube. Although easily visible by eye, the roots within the CT volume present a challenge when it comes to automated segmentation approaches. Conventional approaches of segmenting the roots were tested, such as global thresholding based on greyscale intensity and seeded region-growing approaches. Owing to the voxel intensity variations of the root and their similarity to voxel greyscales in the surrounding soil, these automated approaches were not successful. Automated segmentation of roots from conventional X-ray CT scans is an ongoing challenge; a number of automated and semi-automated approaches have been proposed in other studies [34, 35]. The level of success is case specific with variations in root contrast, spatial resolution, noise, etc. all affecting the capability of these segmentation techniques. To focus the scope of this study, only the three roots circled were segmented manually. Segmentation was performed on every 20th slice (0.92 mm spacing) in the

depth direction. The “Analyze Particles” function in ImageJ [36] was applied to the segmented images on the X-Y plane to obtain the centroids of the root. From this information, the X,Y,Z position of each root was determined.

Figure 10 shows a 3D rendering of the three segmented roots taken at the unloaded (grey) and 20 mm shear displacement stage (red). Part of the benefit of segmenting out the roots is that they can be positioned within the DVC 3D volumetric strain data (Figure 11). This was achieved by importing the segmented root and volumetric 3D strain data into VG studio Max - a 3D volumetric rendering software. Owing to the complexity of the dataset, having the 3D rendering of the roots placed within the 3D strain field aided assessment of the soil-root strain interaction.

To confirm the DVC output results, a direct comparison was made between the local displacements of the root (measured through manual segmentation) against the soil neighbouring the root (measured using DVC). Using the segmented root centroids, the local X-displacements of the root were calculated and plotted as a function of depth. This was directly compared against the neighbouring DVC X-displacements taken three DVC subsets behind the root in the X-direction. The results of this procedure are shown in Figure 12 for each of the seven shear displacement steps. The plots show that the root closely follows the surrounding soil suggesting that the displacement of the root is driven by the deformation of the soil. The similarity in manual segmentation and DVC data gives confidence in the DVC approach for measuring local displacements. The plots in Figure 12 do show some separation between the soil and root over the upper portion of the root (depth position = 45 mm to 60 mm) for displacement steps three and beyond; this was confirmed by studying the region surrounding the root shown in Figure 13.

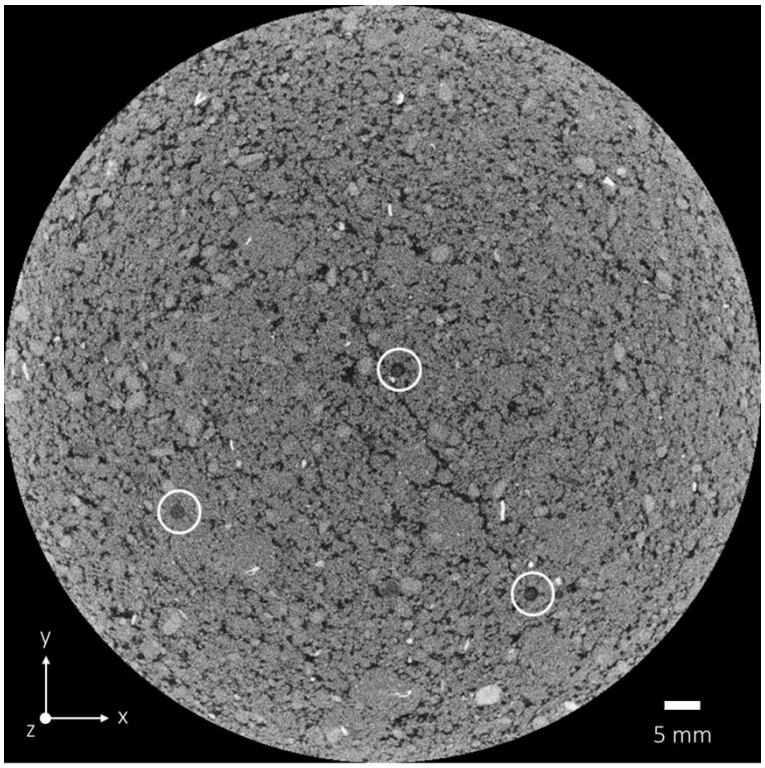

Figure 9: X-ray CT cross-section across the shear plane. Three vertical roots are circled.

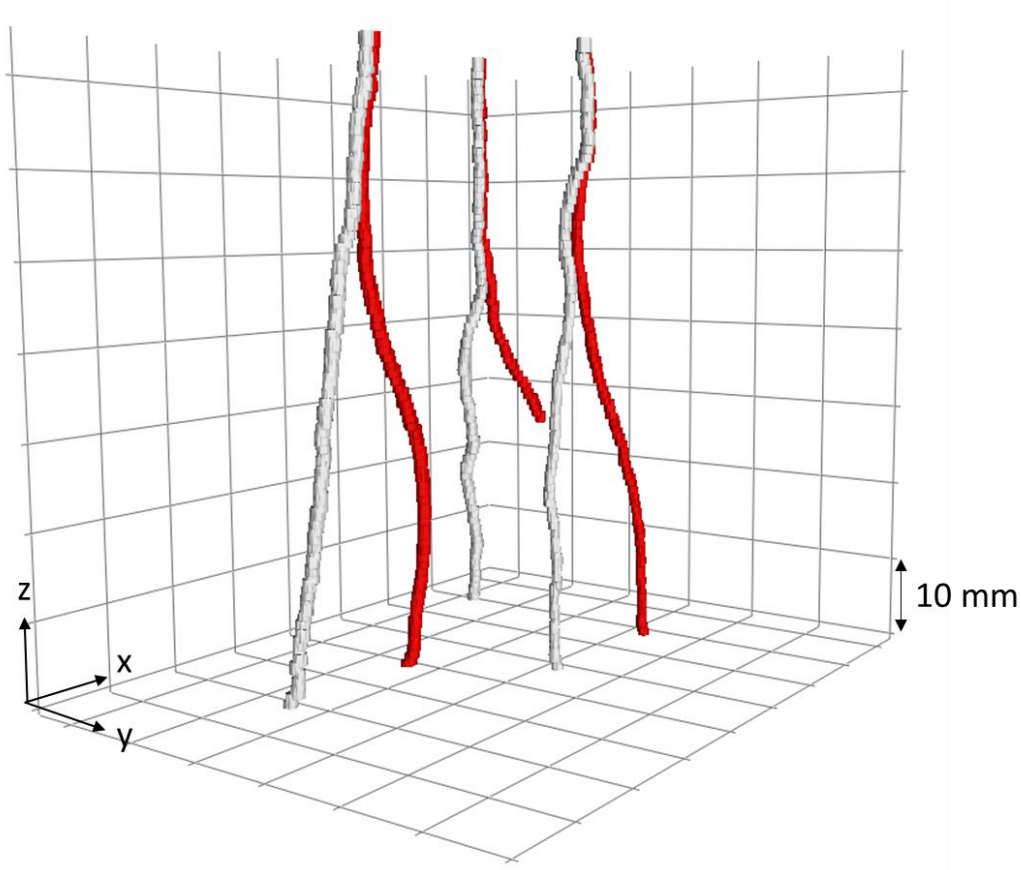

Figure 10: Segmented roots showing the undeformed state (in grey) and deformed state after 20 mm of shear displacement was applied (in red). Shear displacement was applied in the X-direction, with the Z-axis indicating the depth of the tube.

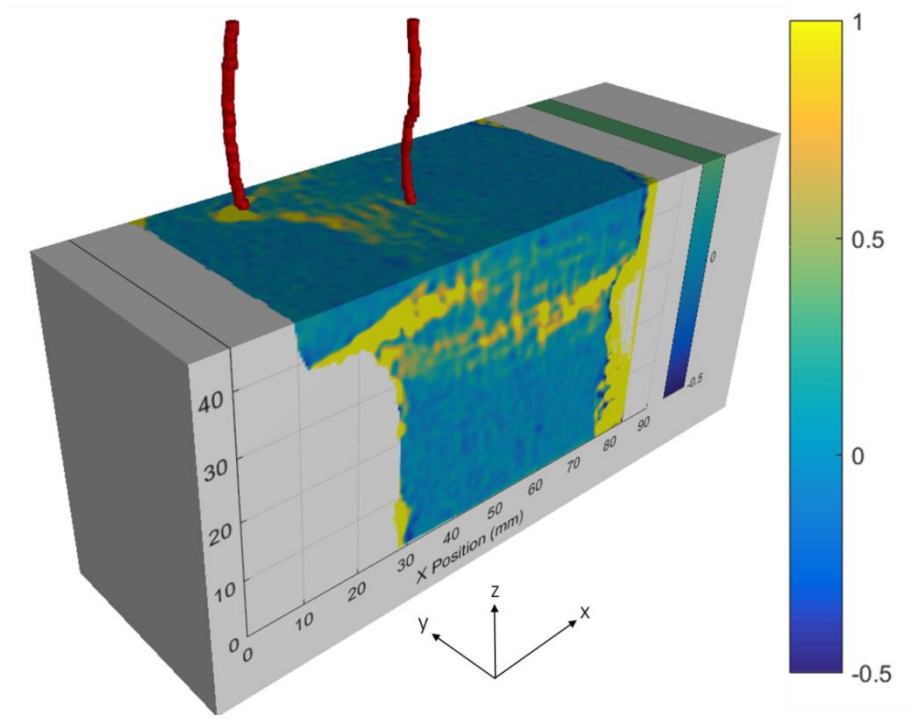

Figure 11: 3D rendering of roots (red) overlaid with 3D volumetric strain data plot mapped to the deformed image.

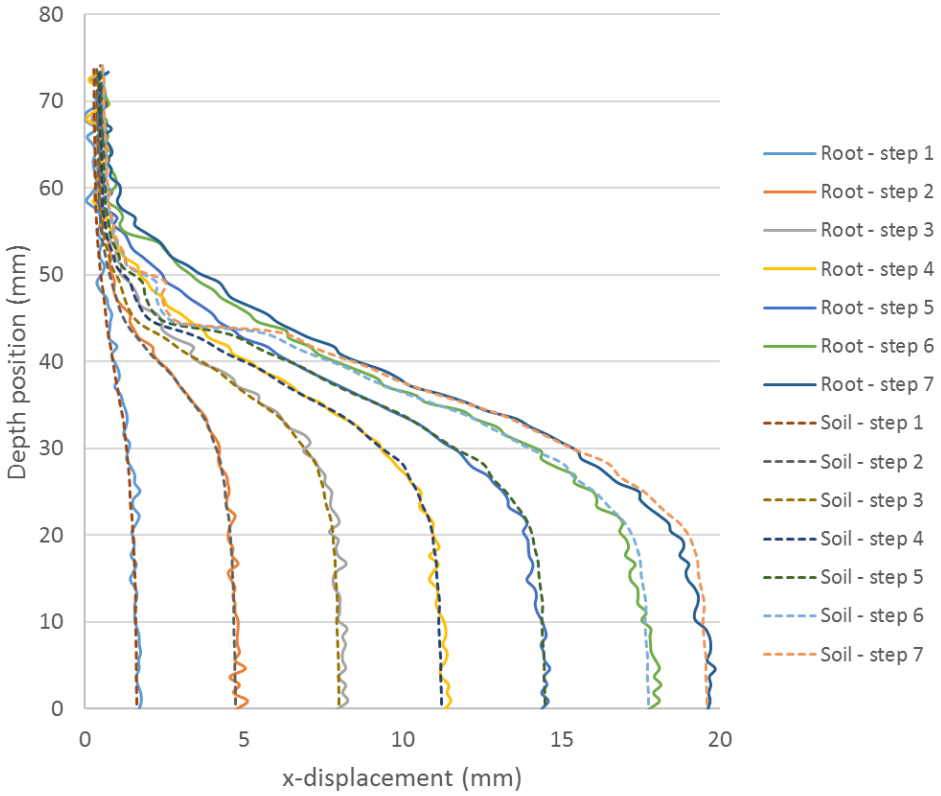

Figure 12: Plots tracking the local change in x-displacement at each displacement step as a function of depth position. Comparisons are made between local x-displacement of the root determined through manual segmentation, and the soil obtained through DVC.

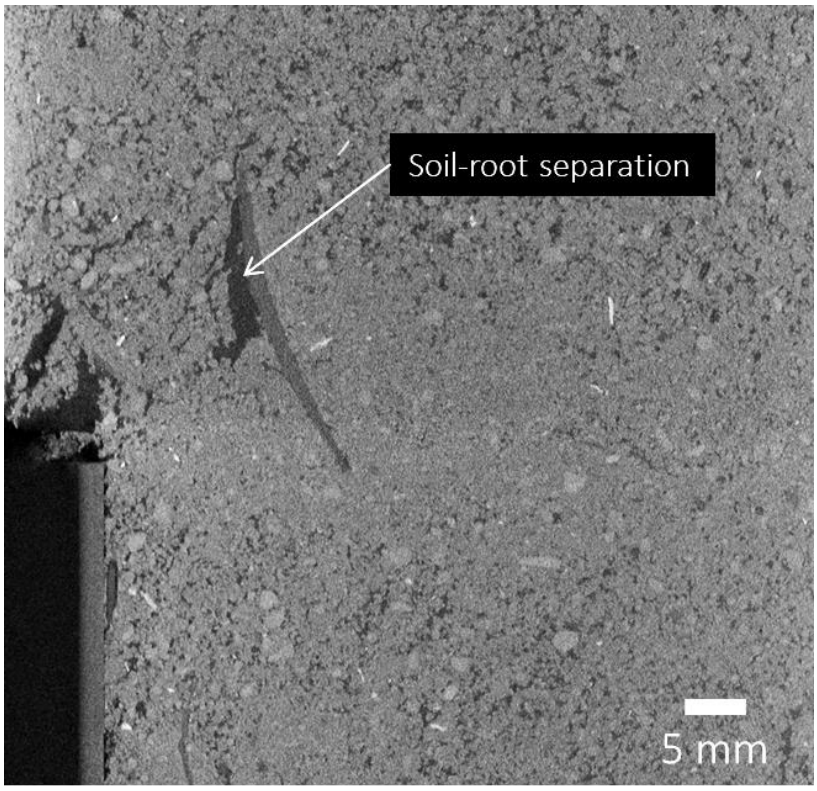

Figure 13: X-ray CT cross-section of root separating from surrounding soil at corner region confirming the soil-root separation behaviour in the plots shown in Figure 12.

The key benefit of using full-field approaches such as DVC is the ability to track local displacement and strain behaviour within a 3D volume. To demonstrate the features captured, Figure 14 shows a cross-sectional full-field map of volumetric strain and ε_{xz} shear strain. The strain map region was placed over the deformed CT cross-section and a Z-projected "thick slice" so that comparisons could be made with local features, a number of which are captured. The use of a thick slice allows features that go into or out the page to be represented on a single projected image. This was generated using the minimum intensity Z-project feature in ImageJ software, and was applied to 100 slices at the root region. This allows the root and crack profiles to be projected onto a single plane for clearer assessment.

Comparing the DVC data with the CT cross-sections in Figure 14 reveals several features. First, the development of cracks adjacent to the boundaries of the specimen leads to a local increase in calculated strain, although this 'strain' is a result of a crack opening displacement rather than genuine strain in the soil. Secondly, the presence of the (stiff) near-vertical root lowers the local magnitude of volumetric and ε_{xz} shear strains, as may be expected. Thirdly, the application of direct shear to the specimen creates a "diamond-shaped" shear zone with its maximum height in the middle of the specimen (x-position = 48 mm). The diamond-shaped shear zone is in agreement with a previous modelling study [37] and is associated with the boundary constraints. The non-uniform shear zone thickness means that analytical modelling approaches to predict rooted soil behaviour such as [38-41], in which a constant shear zone thickness is an input parameter, need to be interpreted carefully and may require future modifications to capture this mechanism.

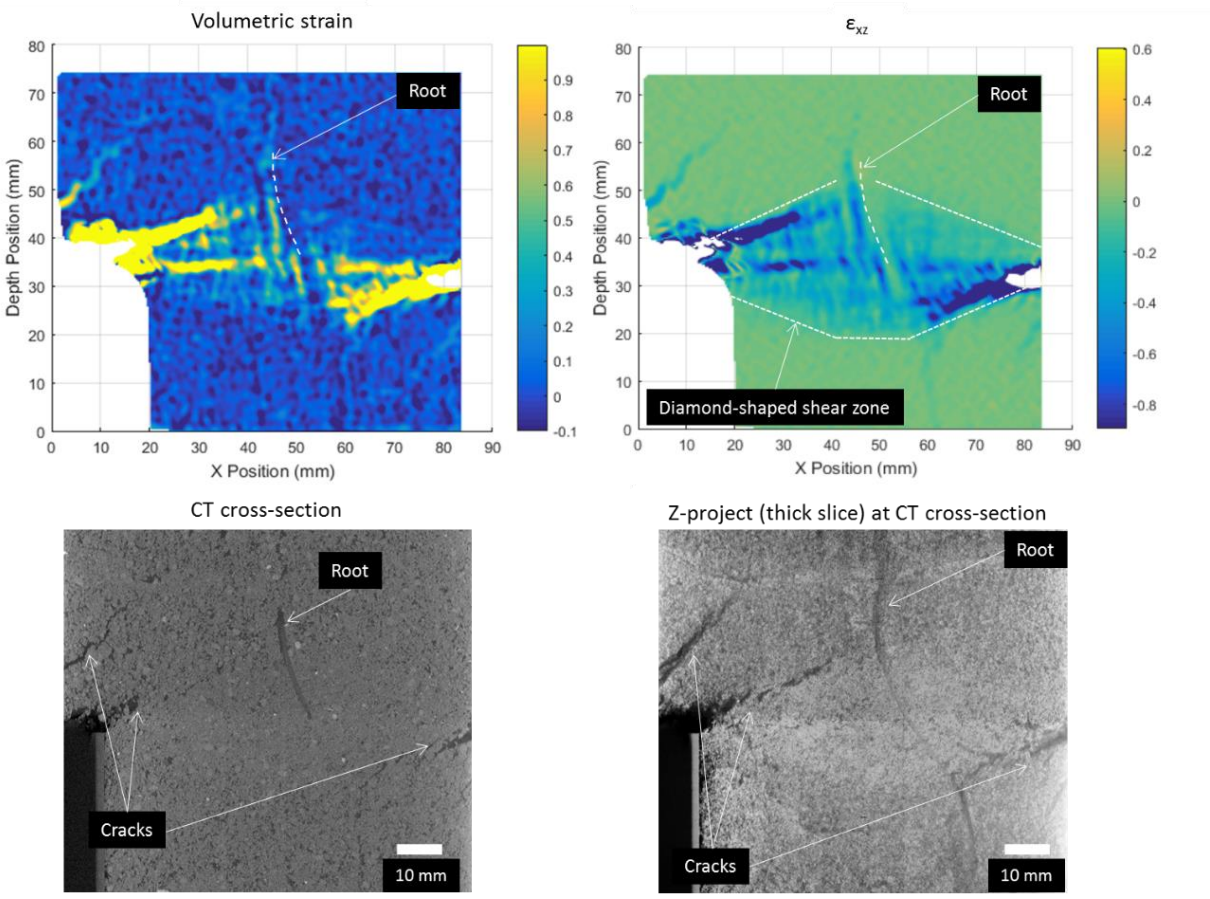

Figure 14: DVC data showing full-field volumetric strain and ε_{xz} shear strain at a cross-section containing a root. For comparison, the X-ray CT cross-section and Z-project (thick slice) at this region are shown.

6.2 Global behaviour

A key challenge with DVC is the large amount of data generated. While it is important to understand the local behaviour of soil, such as local influences between and around individual roots, it is also important to understand the global behaviour of the specimen in shear. The global behaviour can inform the overall performance of different root architectures, root age, and comparisons with unrooted specimens. Global behaviour is also potentially easier to interpret and implement into analytical models. Figure 15 shows displacement and strains averaged over each X-Y slice, plotted as a function of depth from the shear plane. Each X-Y slice was cropped to 40 x 40 mm about the centre of the image to reduce DVC edge effects at the boundaries of the volume.

Several features are identifiable from the global measurements shown in Figure 15. The horizontal displacement plots (Figure 15 a) show the displacement activity and how it develops over each applied displacement step. The horizontal displacement profile is approximately tri-linear with a shear zone developing between +/- 14 mm depth.

The corresponding vertical displacement (Figure 15 b) is most substantial during the first three applied displacement steps (up to a shear displacement of 8.15 mm), after which there are only small changes in vertical soil movement. This behaviour can be explained by soil dilation arising from the fairly dense particle packing, its sand particle content, and the low confining stress [42-44]. Dilation occurs during the initial formation of the shear zone, after which the soil shears at a critical state at (more or less) constant volume. The profile of vertical soil displacement with depth reaches peak magnitudes at depths of -10 and 4 mm from the edges of the shear zone. Outside the shear zone, the vertical displacement starts to decrease towards the top and bottom of the sample.

The remaining plots (Figure 15 c-f) of volumetric, normal ε_{xx}, ε_{zz} and shear ε_{xz} strains respectively show a response contained within the shear zone. The volumetric strain increases in magnitude towards the shear plane, with an increase in volume within this region associated with soil dilation. The largest strain component occurs in the vertical direction, with ε_{zz} reaching a peak normal tensile strain of 75%. In contrast the normal strain ε_{xx}, which acts in the shear displacement direction, is negative indicating compression albeit of a much smaller magnitude (-0.12) than the other components.

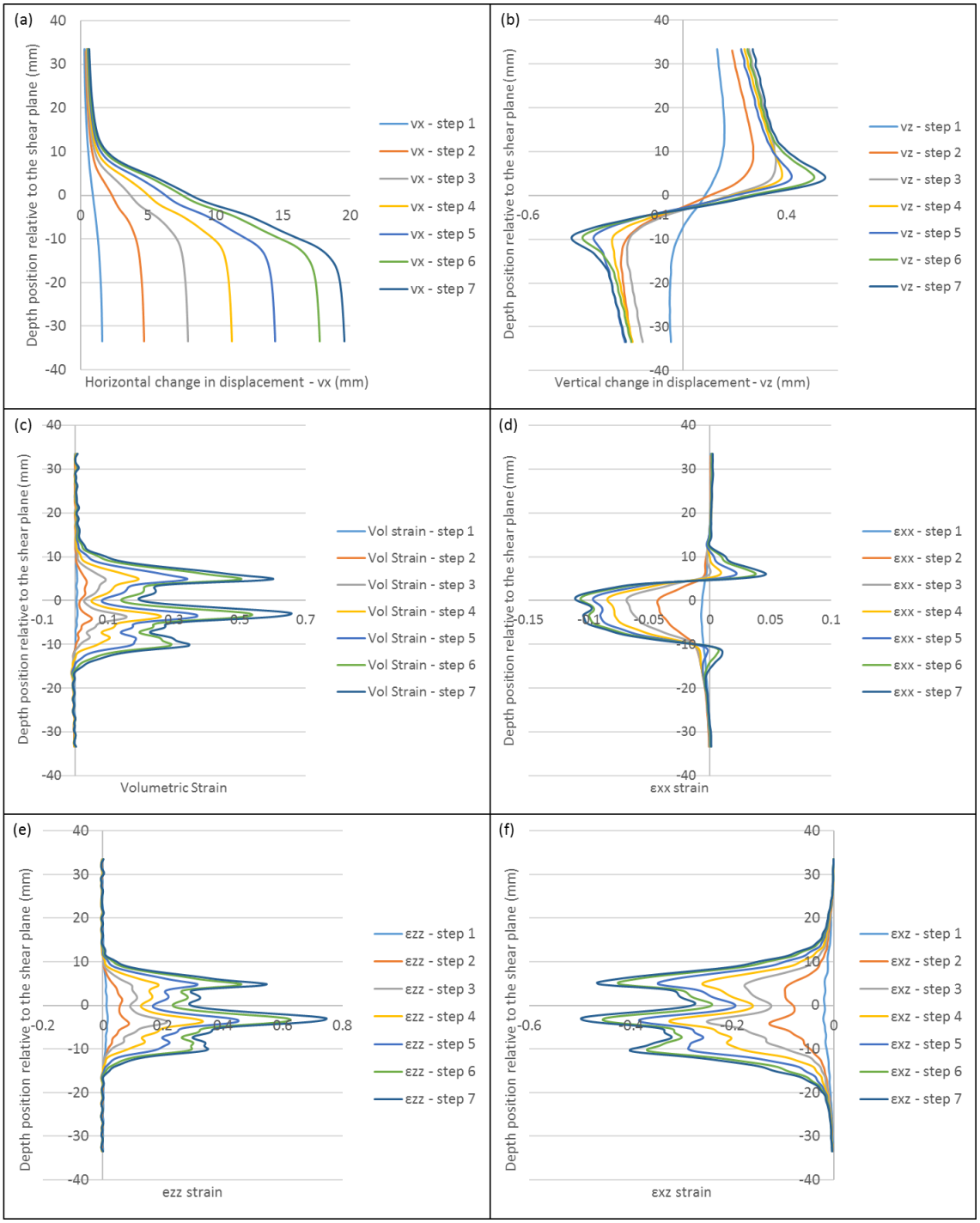

Figure 15: Line plots from DVC dataset showing different parameters plotted against the depth position relative to the shear zone: (a) horizontal X-displacement, (b) vertical displacement, (c) volumetric strain, (d-e) normal strains ε_{xx} and ε_{zz}, and (f) shear strains ε_{xz}.

7 Practical application

Accounting for the effects of vegetation on slope stability is still far from routine in geotechnical engineering, not least because there is a lack of consensus on an acceptable and accepted methodology. The simplest approach, of lowering pore water pressures to account for water removal by plants and adding an empirical effective "cohesion" term to the soil strength to account for the reinforcing effect of roots, is generally held to be over-simplistic and too uncertain [22, 45,

46]. Furthermore, modification of the soil strength and treating the whole as a root-soil composite is conceptually flawed and intellectually unsatisfactory.

More rigorous approaches involve treating the roots, the soil and the pore fluid as separate phases, and considering the forces generated as the roots deform in the analysis of slope equilibrium [17, 38, 39, 47]. One development is to feed the root stress tensor back into the soil to adjust the effective state, allowing a conventional soil behavioural model to be used [38, 39, 48]. Any change in the observed behaviour of the soil is then explained by the changes in its stress state (e.g. an enhanced confining pressure) resulting from the stresses imposed by the roots. Conceptually, this is based on methods of analysis for passive soil reinforcements proposed by Jewell and Wroth [49], Diambra et al. [50], and Ajayi et al. [51]. The additional complication with roots is that they remove water from the soil, affecting the pore water pressure (suction) and the degree of saturation; so ideally, hydraulic as well as mechanical coupling is required [48]. In this way, the effects of differences in degree of saturation and pore water pressure are accounted for through the soil model, rather than through additional artificial or proxy parameters.

Even the more rigorous approach is likely to require a number of simplifications to be made about the behaviour of the roots and the root-soil interface. For example, do the roots only carry tension, or do they have an appreciable bending stiffness and strength? And depending on this, will the root-soil interface fail by relative sliding, or might separation be a kinematically inevitable consequence of the relative deformation? The orientation of the roots relative to a potential shear surface will also have an effect on the shearing resistance that can be mobilised on that surface [38], but a rigorous model that addresses the first two questions reasonably realistically would address this issue automatically. Similarly, the effects of root branching, potential anchorage into the soil by lateral roots, and roots of different stiffness could also be accounted for.

The test methodology developed and demonstrated in this paper provides a way to measure relative soil and root displacement and deformation during shear, giving insights into the real mechanisms of root-soil interaction. These enable the testing of the appropriateness of conceptual behavioural models of root behaviour, for example relating to whether the root bends, stretches or both, remains in contact with the soil, and slippage at the soil-root interface. At the element scale, results from such tests will facilitate the development of new behavioural models, for example the Woodman et al. [48] approach in which the root stress tensor is imposed back into the soil as an effective stress, and the soil then behaves as soil under the root modified stress field. The proposed testing approach could also enable the assumptions and parameters in such a model to be tuned to different root architectures, for example the presence of lateral roots, and roots of different thickness and stiffness. There is still some way from the routine deployment of fully hydro-mechanically coupled models of vegetation in geotechnical slope stability analysis. Nonetheless, the evidence is clear that it will be important to adopt such an approach to make new and existing geotechnical transportation infrastructure affordable, reliable and resilient. This test approach and methodology is an essential step in achieving that goal.

8 Concluding remarks

For the first time, the feasibility of X-ray computed tomography (CT) scanning for an *in situ* direct shear experiment and application of digital volume correlation (DVC) to study full-field displacement and strain information on root-reinforced soil has been demonstrated. Understanding the root-scale soil-root interactions is an essential step in the development and verification of rigorous, bio-hydro-mechanically coupled models for geotechnical slope stability analysis.

In developing and proving the methodology for carrying out these experiments, the following findings and recommendations were established:

1. The *in situ* rig design and scanning procedures need to be carefully considered to give an appropriate trade-off between scan time, signal-to-noise ratio, possible soil movement and spatial resolution.
2. Owing to the large shear displacements (0 to 20 mm) and associated large strains, it is important to have intermediate displacement steps for the DVC process. A step size less than 3.33 mm was shown to work with a "sum of differential approach". The number of displacement steps will however increase the level of noise, which scales with number of steps.
3. It is important to verify the DVC displacement vector fields where possible. This was achieved by comparing local DVC displacement measurements of the soil with local displacements of the root manually segmented from CT images.
4. The DVC subset size has a direct impact on the spatial resolution and level of noise, and scales with the number of displacement steps. Owing to localised strain features in the dataset, a subset size of 32 pixels was chosen. This offered a compromise between strain noise (ε_{xx} standard deviation of 38 millistrain in the final displacement step) and the detectability of localised strain features.
5. The full-field strain maps showed a non-uniform shear zone thickness, with reduction to the shear zone thickness towards the edges of the tube as a result of specimen boundary effects.

9 Acknowledgements

Dr Sonja Schmidt carried out the initial development work on the shear rig, with technical support from Harvey Skinner and Karl Scammell. The authors acknowledge the µ-VIS X-ray Imaging Centre at the University of Southampton for provision of tomographic imaging facilities, supported by EPSRC grant EP/H01506X. All data supporting this study are openly available from the Zenodo data repository [52, 53].

10 Funding statement

This research was funded by the UK Engineering and Physical Sciences Research Council grant numbers EP/M020177/1 and EP/M020355/1, as part of a collaboration between the University of Southampton, University of Dundee, University of Aberdeen, Durham University and the James Hutton Institute. The James Hutton Institute receives funding from the Scottish Government (Rural & Environmental Services & Analytical Services Division).

11 References

[1] Sidle, R.C. & Ochiai, H. 2007 Landslides Processes, Prediction, and Land Use Water Resources Monograph 18. Natural Resources Forum, 322-326.
[2] Gray, D.H. 1995 Influence of Vegetation on the Stability of Slopes. *Vegetation and Slopes*, 2-25.
[3] MacNeil, D., Steele, D., McMahon, W. & Carder, D. 2001 Vegetation for slope stability. In *TRL Report 515*, Crowthorne: Transport Research Laboratory.
[4] Fan, C.C. & Tsai, M.H. 2016 Spatial distribution of plant root forces in root-permeated soils subject to shear. *Soil Till Res* **156**, 1-15. (doi:10.1016/j.still.2015.09.016).
[5] Gonzalez-Ollauri, A. & Mickovski, S.B. 2017 Plant-soil reinforcement response under different soil hydrological regimes. *Geoderma* **285**, 141-150. (doi:10.1016/j.geoderma.2016.10.002).

[6] Veylon, G., Ghestem, M., Stokes, A. & Bernard, A. 2015 Quantification of mechanical and hydric components of soil reinforcement by plant roots. *Can Geotech J* **52**, 1839-1849. (doi:10.1139/cgj-2014-0090).
[7] Liang, T., Bengough, A.G., Knappett, J.A., MuirWood, D., Loades, K.W., Hallett, P.D., Boldrin, D., Leung, A.K. & Meijer, G.J. 2017 Scaling of the reinforcement of soil slopes by living plants in a geotechnical centrifuge. *Ecol Eng* **109**, 207-227. (doi:10.1016.j.ecoleng.2017.06.067).
[8] Comino, E. & Druetta, A. 2010 The effect of Poaceae roots on the shear strength of soils in the Italian alpine environment. *Soil Till Res* **106**, 194-201. (doi:10.1016/j.still.2009.11.006).
[9] Eab, K.H., Likitlersuang, S. & Takahashi, A. 2015 Laboratory and modelling investigation of root-reinforced system for slope stabilisation. *Soils Found* **55**, 1270-1281. (doi:10.1016/j.sandf.2015.09.025).
[10] Mahannopkul, K. & Jotisankasa, A. 2019 Influences of root concentration and suction on Chrysopogon zizanioides reinforcement of soil. *Soils Found* **59**, 500-516. (doi:10.1016/j.sandf.2018.12.014).
[11] Askarinejad, A. & Springman, S.M. 2015 Centrifuge modelling of the effects of vegetation on the response of a silty sand slope subjected to rainfall. *Computer Methods and Recent Advances in Geomechanics*, 1339-1344.
[12] Sonnenberg, R., Bransby, M.F., Hallett, P.D., Bengough, A.G., Mickovski, S.B. & Davies, M.C.R. 2010 Centrifuge modelling of soil slopes reinforced with vegetation. *Can Geotech J* **47**, 1415-1430. (doi:10.1139/T10-037).
[13] Liang, T., Knappett, J.A. & Duckett, N. 2015 Modelling the seismic performance of rooted slopes from individual root-soil interaction to global slope behaviour. *Geotechnique* **65**, 995-1009. (doi:10.1680/geot.14.P.207).
[14] Eab, K.H., Takahashi, A. & Likitlersuang, S. 2014 Centrifuge modelling of root-reinforced soil slope subjected to rainfall infiltration. *Geotech Lett* **4**, 211-216. (doi:10.1680/geolett.14.00029).
[15] Giadrossich, F., Cohen, D., Schwarz, M., Seddaiu, G., Contran, N., Lubino, M., Valdes-Rodriguez, O.A. & Niedda, M. 2016 Modeling bio-engineering traits of Jatropha curcas L. *Ecol Eng* **89**, 40-48. (doi:10.1016/j.ecoleng.2016.01.005).
[16] Leung, F.T.Y., Yan, W.M., Hau, B.C.H. & Tham, L.G. 2015 Root systems of native shrubs and trees in Hong Kong and their effects on enhancing slope stability. *Catena* **125**, 102-110. (doi:10.1016/j.catena.2014.10.018).
[17] Pollen, N. & Simon, A. 2005 Estimating the mechanical effects of riparian vegetation on stream bank stability using a fiber bundle model. *Water Resour Res* **41**, 1-11. (doi:10.1029/2004WR003801).
[18] Ji, X.D., Cong, X., Dai, X.Q., Zhang, A. & Chen, L.H. 2018 Studying the mechanical properties of the soil-root interface using the pullout test method. *J Mt Sci-Engl* **15**, 882-893. (doi:10.1007/s11629-015-3791-4).
[19] Shields, F.D. & Gray, D.H. 1992 Effects of Woody Vegetation on Sandy Levee Integrity. *Water Resour Bull* **28**, 917-931.
[20] Bischetti, G.B., Chiaradia, E.A., Simonato, T., Speziali, B., Vitali, B., Vullo, P. & Zocco, A. 2005 Root strength and root area ratio of forest species in Lombardy (Northern Italy). *Plant Soil* **278**, 11-22. (doi:10.1007/s11104-005-0605-4).
[21] Greenwood, J.R., Norris, J.E. & Wint, J. 2004 Assessing the contribution of vegetation to slope stability. *P I Civil Eng-Geotec* **157**, 199-207.
[22] Wu, T.H. 2013 Root reinforcement of soil: review of analytical models, test results, and applications to design. *Can Geotech J* **50**, 259-274. (doi:10.1139/cgj-2012-0160).
[23] Thakur, V., Nordal, S., Viggiani, G. & Charrier, P. 2018 Shear bands in undrained plane strain compression of Norwegian quick clays. *Can Geotech J* **55**, 45-56. (doi:10.1139/cgj-2016-0443).
[24] Latha, G.M., Vangla, P. & Roy, N. 2018 Image-Based Characterization Techniques for Geotechnical Applications. In *Geotechnics for Natural and Engineered Sustainable Technologies: GeoNEst* (eds. A.M. Krishna, A. Dey & S. Sreedeep), pp. 145-162. Singapore, Springer Singapore.

[25] Keyes, S.D., Gillard, F., Soper, N., Mavrogordato, M.N., Sinclair, I. & Roose, T. 2016 Mapping soil deformation around plant roots using in vivo 4D X-ray Computed Tomography and Digital Volume Correlation. *J Biomech* **49**, 1802-1811. (doi:10.1016/j.jbiomech.2016.04.023).
[26] Hall, S.A., Bornert, M., Desrues, J., Pannier, Y., Lenoir, N., Viggiani, G. & Besuelle, P. 2010 Discrete and continuum analysis of localised deformation in sand using X-ray mu CT and volumetric digital image correlation. *Geotechnique* **60**, 315-322. (doi:10.1680/geot.2010.60.5.315).
[27] Schluter, S., Leuther, F., Vogler, S. & Vogel, H.J. 2016 X-ray microtomography analysis of soil structure deformation caused by centrifugation. *Solid Earth* **7**, 129-140. (doi:10.5194/se-7-129-2016).
[28] Yildiz, A., Graf, F., Rickli, C. & Springman, S.M. 2019 Assessment of plant-induced suction and its effects on the shear strength of rooted soils. *Proceedings of the Institution of Civil Engineers–Geotechnical Engineering*.
[29] Bay, B.K., Smith, T.S., Fyhrie, D.P. & Saad, M. 1999 Digital volume correlation: Three-dimensional strain mapping using X-ray tomography. *Exp Mech* **39**, 217-226.
[30] Rueckel, J., Stockmar, M., Pfeiffer, F. & Herzen, J. 2014 Spatial resolution characterization of a X-ray microCT system. *Appl Radiat Isotopes* **94**, 230-234.
[31] Heeraman, D.A., Hopmans, J.W. & Clausnitzer, V. 1997 Three dimensional imaging of plant roots in situ with x-ray computed tomography. *Plant Soil* **189**, 167-179.
[32] Paulus, M.J., Gleason, S.S., Kennel, S.J., Hunsicker, P.R. & Johnson, D.K. 2000 High resolution X-ray computed tomography: An emerging tool for small animal cancer research. *Neoplasia* **2**, 62-70.
[33] Gillard, F., Boardman, R., Mavrogordato, M., Hollis, D., Sinclair, I., Pierron, F. & Browne, M. 2014 The application of digital volume correlation (DVC) to study the microstructural behaviour of trabecular bone during compression. *J Mech Behav Biomed* **29**, 480-499. (doi:10.1016/j.jmbbm.2013.09.014).
[34] Lafond, J.A., Han, L.W. & Dutilleul, P. 2015 Concepts and Analyses in the CT Scanning of Root Systems and Leaf Canopies: A Timely Summary. *Front Plant Sci* **6**. (doi:10.3389/Fpls.2015.01111).
[35] Tabb, A., Duncan, K.E. & Topp, C.N. 2018 Segmenting root systems in X-ray computed tomography images using level sets. *IEEE Wint Conf Appl*, 586-595. (doi:10.1109/Wacv.2018.00070).
[36] Rueden, C.T., Schindelin, J., Hiner, M.C., DeZonia, B.E., Walter, A.E., Arena, E.T. & Eliceiri, K.W. 2017 ImageJ2: ImageJ for the next generation of scientific image data. *Bmc Bioinformatics* **18**.
[37] Wang, J., Dove, J.E. & Gutierrez, M.S. 2007 Discrete-continuum analysis of shear banding in the direct shear test. *Geotechnique* **57**, 513-526.
[38] Wu, T.H., McKinnell Iii, W.P. & Swanston, D.N. 1979 Strength of tree roots and landslides on Prince of Wales Island, Alaska. *Can Geotech J* **16**, 19-33. (doi:10.1139/t79-003).
[39] Waldron, L.J. 1977 The Shear Resistance of Root-Permeated Homogeneous and Stratified Soil1. *Soil Science Society of America Journal* **41**, 843-849. (doi:10.2136/sssaj1977.03615995004100050005x).
[40] Gray, D.H. & Ohashi, H. 1983 Mechanics of Fiber Reinforcement in Sand. *J Geotech Eng-Asce* **109**, 335-353.
[41] Meijer, G.J., Muir Wood, D., Knappett, J.A., Bengough, A.G. & Liang, T. 2019 Root branching affects the mobilisation of root-reinforcement in direct shear. *E3S Web Conf.* **92**, 12010.
[42] Simoni, A. & Houlsby, G.T. 2006 The direct shear strength and dilatancy of sand–gravel mixtures. *Geotechnical & Geological Engineering* **24**, 523.
[43] Farhadi, B. & Lashkari, A. 2017 Influence of soil inherent anisotropy on behavior of crushed sand-steel interfaces. *Soils Found* **57**, 111-125. (doi:10.1016/j.sandf.2017.01.008).
[44] Houlsby, G.T. 1994 How the Dilatancy of Soils Affects Their Behaviour. *Deformation of Soils and Displacements of Structures - X Ecsmfe, Vol 4*, 1189-1202.
[45] Wilkinson, P.L., Anderson, M.G. & Lloyd, D.M. 2002 An integrated hydrological model for rain-induced landslide prediction. *Earth Surf Proc Land* **27**, 1285-1297. (doi:10.1002/esp.409).
[46] Ni, J.J., Leung, A.K., Ng, C.W.W. & Shao, W. 2018 Modelling hydro-mechanical reinforcements of plants to slope stability. *Comput Geotech* **95**, 99-109. (doi:10.1016/j.compgeo.2017.09.001).

[47] Pollen-Bankhead, N. & Simon, A. 2009 Enhanced application of root-reinforcement algorithms for bank-stability modeling. *Earth Surf Proc Land* **34**, 471-480. (doi:10.1002/esp.1690).
[48] Woodman, N.D., J.A., S., Roose, T., Powrie, W., Meijer, G.J., Knappett, J.A. & Dias, T. 2020 Mathematical and computational modelling of vegetated soil incorporating hydraulically-driven finite strain deformation. *Manuscript submitted for publication.*
[49] Jewell, R.A. & Wroth, C.P. 1987 Direct Shear Tests on Reinforced Sand. *Geotechnique* **37**, 53-68. (doi:10.1680/geot.1987.37.1.53).
[50] Diambra, A., Ibraim, E., Wood, D.M. & Russell, A.R. 2010 Fibre reinforced sands: Experiments and modelling. *Geotext Geomembranes* **28**, 238-250. (doi:10.1016/j.geotexmem.2009.09.010).
[51] Ajayi, O., Le Pen, L., Zervos, A. & Powrie, W. 2017 A behavioural framework for fibre-reinforced gravel. *Geotechnique* **67**, 56-68. (doi:10.1680/jgeot.16.P.023).
[52] Bull, D.J., Smethurst, J.A., Sinclair, I., Fabrice, P., Roose, T., Powrie, W. & Bengough, A.G. 2020 Noise study data for: Mechanisms of root-reinforcement in soils: an experimental methodology using 4D X-ray computed tomography and digital volume correlation. Zenodo Digital Repository.(doi:10.5281/zenodo.3361832).
[53] Bull, D.J., Smethurst, J.A., Sinclair, I., Fabrice, P., Roose, T., Powrie, W. & Bengough, A.G. 2020 Data for: Mechanisms of root-reinforcement in soils: an experimental methodology using 4D X-ray computed tomography and digital volume correlation. Zenodo Digital Repository.(doi:10.5281/zenodo.3352268).